

Chapter 10

Visualization of Functional Structure and Kinetic Dynamics of Cellulases



Akihiko Nakamura and Ryota Iino

Abstract Cellulose is the most abundant carbohydrate on earth and hydrolyzed by cellulases in nature. During catalysis, cellulase transfers protons to and from the oxygen atoms of the glycosidic bond and a water molecule. Since cellulose is an insoluble polymer, some kinds of cellulases, with high activity toward crystalline cellulose, move on the crystal surface with continuous hydrolysis of the molecular chain. In addition, binding and dissociation on/from the crystal surface are also important elementary steps of the reaction cycle. Recently, these interesting features of cellulases can be directly analyzed, due to the development of visualization techniques. In this chapter, we introduce (1) visualization of the protonation state of the catalytic residue by neutron crystallography, (2) visualization of processive movement on the crystal surface by high-speed atomic force microscopy, and (3) visualization of binding and dissociation events by single-molecule fluorescence microscopy.

Keywords Cellulase · cellulose · Processivity · Molecular motor · Single-molecule analysis · Neutron crystallography · Proton pathway

A. Nakamura (✉)

Okazaki Institute for Integrative Bioscience, National Institutes of Natural Sciences, Aichi, Japan

Department of Functional Molecular Science, School of Physical Sciences, Kanagawa, Japan
e-mail: aki-naka@ims.ac.jp

R. Iino

Okazaki Institute for Integrative Bioscience, National Institutes of Natural Sciences, Aichi, Japan

Department of Functional Molecular Science, School of Physical Sciences, Kanagawa, Japan
Institute for Molecular Science, National Institutes of Natural Sciences, Aichi, Japan

10.1 Introduction

Cellulase hydrolyzes cellulose, the main component of plant cell walls, to mono- or oligosaccharides. Cellulase is mainly produced by fungi and bacteria that live in soil (Štursová et al. 2012), coexist with animals (Julliard et al. 1999), or are pathogens of plants (Wood 1960). Cellulases are classified as members of the glycoside hydrolase (GH) family based on amino acid sequences and three-dimensional structures in the Carbohydrate-Active enZymes (CAZy) database (Lombard et al. 2014). At this time (Feb., 2018), 149 GH families exist, and cellulases are classified in 12 families (GH5, 6, 7, 8, 9, 12, 44, 45, 48, 51, 74, and 124). Traditional classifications of them, based on activity, are cellobiohydrolases and endoglucanases (EC 3.2.1.4). The former is additionally separated into nonreducing-end cellobiohydrolases (EC 3.2.1.91) and reducing-end cellobiohydrolases (EC 3.2.1.176), depending on different preferences for the ends of the molecular chain (Fig. 10.1). Cellobiohydrolases mainly produce cellobiose (a β -1,4-linked glucose dimer) from chain ends, and endoglucanase cuts the middle of chains in amorphous regions. Many cellulases consist of a catalytic domain (CD) and a cellulose-binding domain (CBD). These two domains of fungal cellulases are connected by an intrinsically disordered region modified with sugars, and those of bacterial cellulase (Leschine 1995) are connected by linker domain (i.e., fibronectin type III-like domain). Although, cellulases without CBD also exist. In this chapter, we focus on fungal cellulase.

Two reaction mechanisms have been proposed for cellulases depending on the anomeric structure of the products: one is the retaining mechanism, and the other is the inverting mechanism (McCarter and Stephen Withers 1994). In the former case, the catalytic nucleophile residue attacks the C1 carbon of glucose, and the catalytic acid/base residue protonates the oxygen of the glycosidic bond. After making a glycosyl-enzyme intermediate, the catalytic acid/base residue receives a proton from a water molecule, and the glycosidic bond of the intermediate is hydrolyzed.

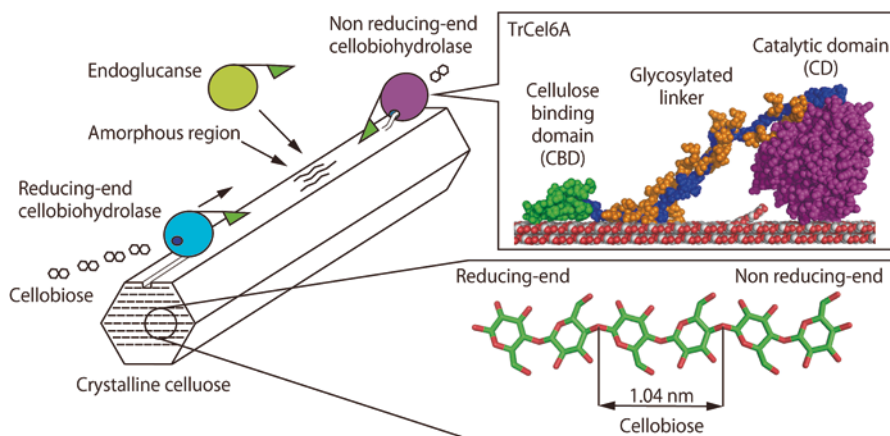


Fig. 10.1 Structure of cellulose and the domain construction of cellulase

On the other hand, inverting cellulases hydrolyze cellulose at once with protonation of the oxygen of the glycosidic bond and activation of water by the catalytic acid and base residues, respectively. Both mechanisms basically need two acidic residues (aspartate or glutamate) and catalyze proton exchanges between cellulose and water molecules. Therefore, visualization of the protonated states of the residues around the substrate-binding site is useful to determine the catalytic residues and mechanisms.

The most unique feature of cellulase is the heterogeneous reaction at the liquid-solid interface. Cellulose is an insoluble polymer of β -1,4-linked glucose, and the molecular chains make stable crystal structures. During the reaction, cellulase needs to bind on the surface of cellulose, hydrolyze the glycosidic bond, and dissociate from the surface. In the case of crystalline cellulose hydrolysis, not all enzyme-binding events are productive, because molecular chains are tightly packed and hydrolyzable parts are limited (Jalak et al. 2012). The constants (e.g., turnover and dissociation constant) obtained by biochemical assays are averages of all states. Therefore, single-molecule analysis is needed to determine the binding rate constant (k_{on}), dissociation rate constant (k_{off}), and turnover of “truly” productive molecules. Actually, the movement of cellobiohydrolases on crystalline cellulose that had been expected from biochemical results was directly visualized by high-speed atomic force microscopy (HS-AFM), as described below (Igarashi et al. 2009).

In this chapter, we will introduce visualization of (1) protonation states of the catalytic residue by neutron and X-ray crystallography, (2) processive movement by HS-AFM, and (3) binding and dissociation on/from cellulose crystals by single-molecule fluorescence microscopy. These visualization methods should be useful not only for the characterization of cellulases but also for other carbohydrate active enzymes.

10.2 Visualization of Protonated States by X-Ray and Neutron Crystallography

The hydrogen atom is the most abundant atom in an enzyme molecule. Hydrogen atom is an important element of hydrogen bonding that is indispensable for stabilization of higher-order enzyme structures and interactions between enzymes and substrates. It is also well known that proton exchange (hydrogen nucleus, generally also called a hydrogen ion or proton) occurs between substrate or solvent and amino acids that have polar groups. Structural analysis, including hydrogen atoms and protons, is extremely important for understanding the structure and reaction mechanism of enzymes.

10.2.1 Advantages and Challenges of Neutron Crystallography

In terms of three-dimensional structure determination of an enzyme, the most common method is X-ray crystallography, and over 100,000 structures have been registered in the Protein Data Bank (PDB), to date. In X-ray crystallography, the electron density of the atoms constituting the enzyme molecule are observed using X-ray as a probe. Carbon, oxygen, and nitrogen atoms that have a large atomic number and a large number of electrons are easily observed, compared to hydrogen atoms. Ultrahigh (sub-angstroms) resolution is needed for observing hydrogen atom, hydride, or proton with coordinate bond (Ogata et al. 2015). On the other hand, neutron crystallography uses neutron as a probe, and neutrons diffracted by nuclei are observed. Therefore, the visibilities of atoms are completely different from X-ray crystallography, as shown in Fig. 10.2 (Varley 1992; McMaster et al. 1969). For example, sulfur atoms, easily observed by X-ray crystallography, show weak scattering intensity in neutron crystallography. Additionally, oxygen and nitrogen atoms are easily distinguished from each other by neutron crystallography because nitrogen atoms clearly show stronger scattering intensity. The most interesting feature of neutron crystallography is the differences of scattering intensities between isotopes. Due to this property, a deuterium atom (D) shows a scattering intensity equivalent to that of carbon atoms, whereas a hydrogen atom (H) shows an apparent negative scattering intensity, because the phase of the scattered neutron is reversed. If the hydrogen atoms of an enzyme are fully exchanged to deuterium atoms, the protonation states of the targeted residues can be easily visualized. During the diffraction measurement, the enzyme crystal will not be damaged or reduced even at room temperature. The energy of the neutron beam of 81.8 meV (7.9 kJ/mol) for a wavelength of 1 Å is not enough to cleave the covalent bonds of amino acids. This is the other advantage of neutron crystallography.

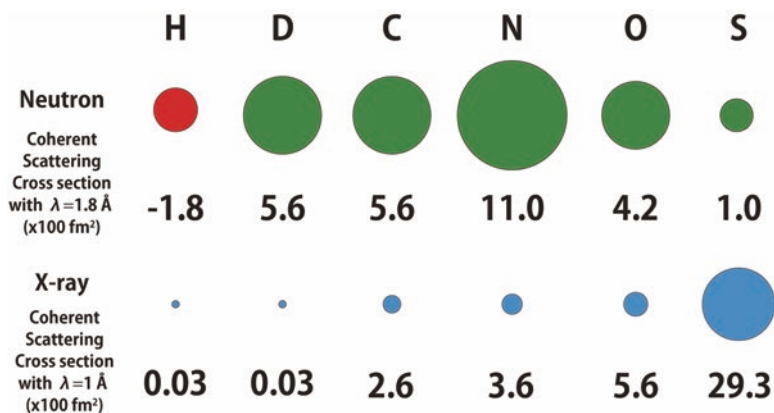


Fig. 10.2 Difference in scattering efficiency among atoms in neutron and X-ray crystallography

There are two types of neutron sources for neutron crystallography. One is a nuclear reactor, which generates a mixed wavelength neutron beam, and the desired wavelength of the neutron beam is separated by a monochromator. This type of sources is available in Japan (Japan Research Reactor No.3), France (High-Flux Reactor), Germany (Forschungs-Neutronenquelle Heinz Maier-Leibnitz), and the USA (High Flux Isotope Reactor). The other is a short-pulsed nuclear spallation neutron source that generates a neutron from nuclear fission of a metal target (such as tungsten or liquid mercury) by pulsed proton beams from a synchrotron or linear accelerator. The neutron wavelength diffracted by the crystal can be selected using a synchronized chopper, because the timing of neutron generation is known. These sources are now available in Japan (Materials and Life Science Experimental Facility; MLF), the United Kingdom (ISIS spallation neutron source), and the USA (Spallation Neutron Source and Protein Crystallography Station). Additionally, a European Spallation Source is under construction in Sweden. Especially for the MLF BL02 iBIX of the Japan Proton Accelerator Research Complex (J-PARC), detectors synchronized with the neutron generator and chopper are used to analyze diffraction spots by a time-resolved Laue method. This system showed one of the highest efficiencies of measurement in the world (Kusaka et al. 2013).

Even with the continuous development of neutron crystallography, the biggest problem is the weak brightness of the neutron source. Because of this disadvantage, usually more than 1 mm³ of protein crystal and a half-month of measurement are needed for diffraction analysis. The probability of big crystal formation can be increased with detailed analysis of the crystallization condition (Nakamura et al. 2013a), but crystal preparation is still the bottleneck of neutron crystallography. Further improvement of facilities and crystallization techniques are necessary to make neutron crystallography more generalized.

10.2.2 An Example of Protonation Analysis of Cellulase

Some cellulases do not have a pair of acidic residues at the expected catalytic site from substrate-bound structures. For example, a GH45 inverting cellulase from a basidiomycete *Phanerochaete chrysosporium* (PcCel45A) has an aspartic acid residue as the catalytic acid and produces products from cellulose, but an acidic residue was not found at a suitable position for the catalytic base residue (Nakamura et al. 2015). The asparagine 92 residue was identified as a possible catalytic base from structural comparison with the most studied GH45 cellulase from the ascomycete *Humicola insolens* (HiCel45A) (Fig. 10.3a). In a biochemical assay, the PcCel45A N92D mutant showed drastically lower activity than the WT, indicating that Asn92 is acting as the catalytic residue (Fig. 10.3b). These results mean that PcCel45A has a different mechanism from other known cellulases. Normally, however, asparagine cannot receive a proton at a moderate pH, because protonation of nitrogen and oxygen atoms at a side chain amide need pH -7 or pH 0, respectively. Therefore, neutron crystallography was applied to determine the protonation states of Asn92 and

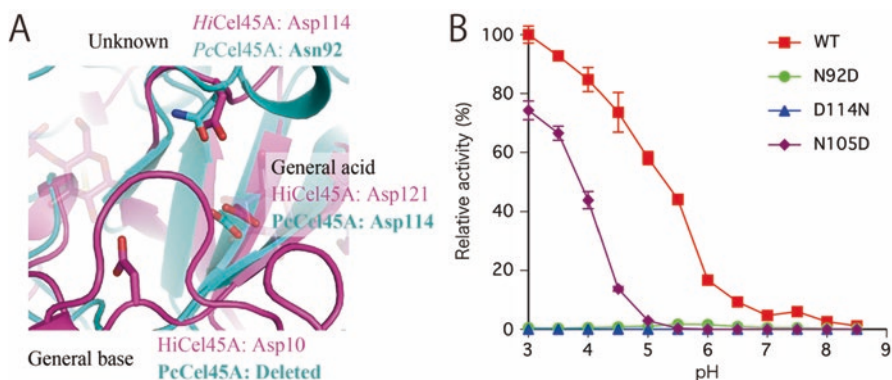


Fig. 10.3 (a) Superposition of the active sites of PcCel45A and HiCel45A (b) pH dependencies of the activity of PcCel45A WT, D114A, N92D, and N105D

the reaction mechanism of PcCel45A. Neutron diffraction from the 6 mm³ crystal was measured for 13.5 days at the iBIX in the MLF of J-PARC with 300 kW accelerator power. As a result, it was revealed that the Asn92 residue is not in the usual “amide form,” but in the “imidic acid form,” that is, the tautomer of amide (Fig. 10.4). However, under normal conditions, the imidic acid form is unstable, and the equilibrium is biased to the amide form. Then, further analysis of the hydrogen bond around the catalytic residue revealed that the oxygen of the carbonyl of the Asn92 side chain and the nitrogen of the amide of the main chain are connected by the positive scattering power map of neutron crystallography. Since no scattering map was observed there with X-ray crystallography, it was expected that deuterium ion was shared between the two atoms. Next, the hydrogen bonds between the two catalytic residues (Asn92 and Asp114) were also analyzed in detail, and it was confirmed that the two catalytic residues are connected by a series of the positive scattering power map of neutron (Fig. 10.4). To verify these results, the activity profile of PcCel45A N105D was analyzed, because Asn105 does not directly participate in substrate recognition or catalysis itself, but it looks to be relaying protons between the catalytic residues. As expected, the N105D mutant retained 80% activity, compared to wild type at pH 3.0, whereas at pH 5.5, the activity of the N105D mutant was completely lost (Fig. 10.3b). This is likely because the proton relay pathway is disconnected, due to the deprotonation of the aspartic acid side chain (pK_a 3.9) at a lower pH than the wild type. From these results, it was shown that PcCel45A uses the imidic acid form of Asn92 as the catalytic base and that protonation of the glycosidic bond and activation of the water molecule is coupled to the proton pathway. In this model, the imidic acid form of Asn92 can be regenerated via reverse proton relays by protonation of Asp114; thus it can be explained why the optimal pH of the reaction is acidic.

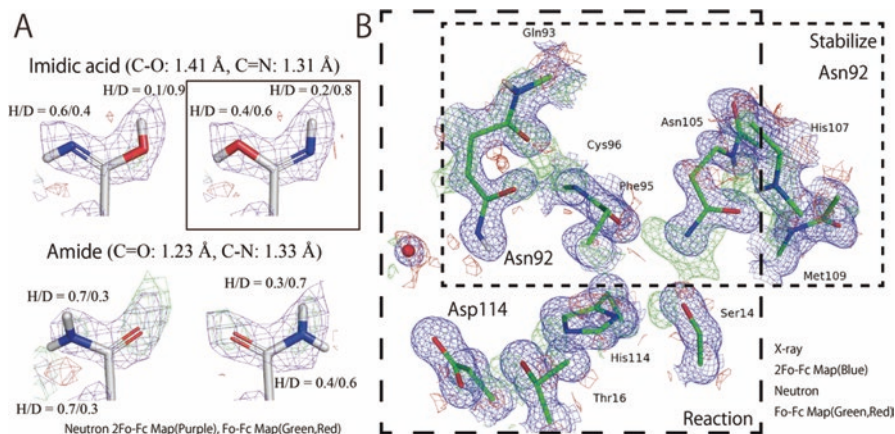


Fig. 10.4 (a) Imidic acid form of Asn92 in PcCel45A WT. (b) Neutron scattering power map between Asn92 and Asp114

10.3 Visualization of Processive Movement of Cellulase by HS-AFM

High-speed atomic force microscopy (HS-AFM) is the cutting-edge technique in single-molecule observation. The most important point of this system is that enzymes can be visualized without labeling. Higher frame rates and lower tapping force than conventional AFM were achieved using small cantilevers and high-speed scanners (Ando 2013). Actually, unidirectional movement of myosin V on actin filaments (Kodera et al. 2010) and chitinase on the crystal chitin surface (Igarashi et al. 2014) was visualized. In addition, the structural change of bacteriorhodopsin with photo activation (Shibata et al. 2010) and cooperative movements of the ring of a rotating motor F_1 -ATPase ($\alpha_3\beta_3$ subunits), without the rotator (γ -subunit), were observed (Uchihashi et al. 2011). Recently, the distance distribution between two domains, connected by an intrinsically disordered region, was also analyzed (Kodera et al. 2015). These results mean that even the structural dynamics of enzymes can be visualized by HS-AFM. Please read reviews by developers about the detailed working mechanism of HS-AFM (Ando 2017).

One of the most exciting findings in the cellulase research is the direct observation of the processive movement of GH7 cellobiohydrolase from the ascomycete *Trichoderma reesei* (TrCel7A) using HS-AFM (Igarashi et al. 2009), like shown in Fig. 10.5. As described as above, cellobiohydrolases have been thought of as processive enzymes, because they specifically produce cellobioses, that is, the repeating unit of the cellulose molecular chain. From the structural comparison between cellobiohydrolase and endoglucanase in the same GH family, it was shown that only cellobiohydrolases have a tunnelloike structure to keep the substrate-bound state

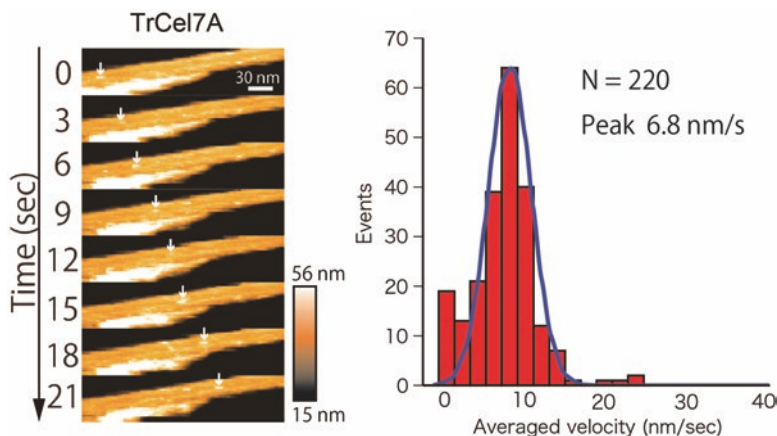


Fig. 10.5 Processive movement of TrCel7A observed by HS-AFM

(Davies and Henrissat 1995). Furthermore, sharpened edges of cellulose crystals, after degradation by cellobiohydrolases, were shown by electron microscopy (Imai et al. 1998). Processivity of cellulases have been discussed for a long time with these indirect evidences. Visualization of processive movement by HS-AFM provided a new direction of analysis for cellulase characterization, like moving velocity (meaning k_{cat} of a productive molecule) and moving length (indicating processivity).

10.3.1 Analysis of Velocity and Processivity by HS-AFM

For the observation of cellulase movement, cellulose crystals should be stabilized on the surface of a graphite disc or hydrophobized mica, stuck on a glass stage. Fortunately, cellulose crystals are bound on their surface by just putting a drop of the cellulose crystal suspension, because a cellulose crystal has hydrophobic planes on its surface. Usually, 2 μl of 20 μM enzyme are added into 80 μl of observation buffer in the liquid chamber. In the case of a weak-binding mutant, like a separated CD, about ten times higher concentration of enzyme solution is required to find moving molecules. The highest frame rate reported previously is 5 fps. Higher frame rates will provide better time resolution for moving time analysis and processivity estimation, but they also make it difficult to track moving molecules across a long distance, due to the limitation of the field of view. Tracking of moving molecules is achieved by peak estimation with a 2D-Gaussian distribution fitting to the molecule image of height per frame. Moving distance and time are calculated from the difference of peak positions and number of frames between the start and end frames of movement. From these values, velocities of each molecule are determined, and the moving velocity of the enzyme can be estimated from the

distributions of these velocities of observed molecules. In single-molecule analysis, a velocity of an observed molecule does not always represent the typical character of the target enzyme, because the values of the velocities of molecules follow a Gaussian distribution, if the enzyme has a single mode of movement. Therefore, velocities of a high enough number of molecules should be analyzed to discuss the overall enzyme properties. The analysis of moving time follows the same manner. Distribution of moving times of observed molecules is fitted with an exponential decay function, and moving time (or dissociation constant) can be determined. Moving distance can be calculated using the values of velocity and moving time, and processivity can be calculated when the step size of cellobiohydrolases is assumed as 1 nm from the size of cellobiose (1.04 nm).

Not many kinds of cellobiohydrolases were observed with HS-AFM. Values of velocity and processivity have only been compared among TrCel7A and two isozymes of GH7 cellobiohydrolases from *P. chrysosporium* (PcCel7C and PcCel7D) (Nakamura et al. 2014). All of them hydrolyze cellulose from reducing ends. At first, the processive movement of TrCel7A was compared, across the wild-type enzyme, only the CD, an inactive mutant (E212Q) and a less-active mutant to crystalline cellulose (W40A) (Igarashi et al. 2009). Processive movement of the TrCel7A CD indicated that the CBD and linker region are not necessary for processive movement. On the other hand, TrCel7A E212Q just bound to cellulose and did not move. From these results, it was clearly shown that TrCel7A moves on cellulose with hydrolysis of the chain. Additionally, processive movement of TrCel7A W40A was also not found, although Trp40 is only located at the entrance of the tunnel structure and far from the catalytic site. The tryptophan residue at the entrance of the tunnel is highly conserved in GH7 cellobiohydrolases (Nakamura et al. 2013b). In a biochemical assay, TrCel7A W40A showed lower activity per bound enzyme to crystalline cellulose, but higher specific activity toward amorphous cellulose. The role of Trp40 in TrCel7A was identified from the results of molecular dynamics simulations. When the glucose ring of the reducing end of the cellulose chain was placed on Trp40, wild-type TrCel7A can take the molecular chain into the tunnel-like structure. In contrast, W40A could not hold the reducing end at the entrance of the tunnel and failed to take in the chain. However, when the chain end was placed in the tunnel, there was no difference between the wild type and W40A, indicating that Trp40 is just important for initial chain catching at the entrance of the tunnel. Trp40 is important only for crystalline cellulose degradation, because the number and length of available chain ends might be limited on the surface of crystalline cellulose, compared to disordered amorphous cellulose.

Compared to cellobiohydrolases from *Ascomycetes* like TrCel7A, cellobiohydrolases from *Basidiomycetes* have more open tunnel structures, due to the deletion of loops (Nakamura et al. 2014). These structural features are expected to cause the difference in processivities, but there has been no clear evidence. In a direct comparison of the processive movement with HS-AFM, the processivity of TrCel7A was 34.0, while the processivities of PcCel7D and PcCel7C were 29.4 and 28.8, respectively (Table 10.1). TrCel7A showed higher processivity than PcCel7D and PcCel7C, as expected. Their moving times showed a similar trend, and the values

Table 10.1 Moving velocities, moving time, and processivity of GH7 cellobiohydrolases

Enzyme	Velocity (nm/s)	Moving time (s)	Processivity
TrCel7A	6.8 ± 3.5	3.5 ± 0.2	34.0
PcCel7D	9.4 ± 3.7	2.2 ± 0.1	29.4
PcCel7C	14.7 ± 9.1	1.4 ± 0.0	28.8

From Nakamura et al. (2014)

were 5.0 s (TrCel7A), 3.1 s (PcCel7D), and 2.0 s (PcCel7C). Interestingly, the order of moving velocities was opposite, and TrCel7A showed the slowest velocity (6.8 nm/s) in the three. The velocity of PcCel7C (14.7 nm/s) was higher than that of PcCel7D (9.4 nm/s). This trade-off relationship between velocity and processivity, or moving time, indicates that a high affinity to the cellulose chain causes slow-moving actions. These results show that HS-AFM is a powerful tool to analyze the relationship between structure and function of processive cellobiohydrolases.

One of the GH6 cellobiohydrolases from *T. reesei* (TrCel6A) that hydrolyzes cellulose from nonreducing ends was also observed by HS-AFM (Igarashi et al. 2011), but clear movement of TrCel6A was not observed, even though TrCel6A showed crystals with sharpened edges in electron microscopy analysis (Chanzy and Henrissat 1985). Some GH6 enzymes from cellulose-degrading bacterial species showed processive motion on cellulose crystals, but this has not yet been published. Further analysis is needed to clarify the structural and functional differences of moving and nonmoving GH6 cellobiohydrolases in HS-AFM observation.

10.4 Visualization of Binding and Dissociation by Single-Molecule Fluorescence Microscopy

Single-molecule fluorescence microscopy is a more conventional method than HS-AFM, but it is still a very useful technique (Iino et al. 2017). To visualize target molecules, samples must be labeled with fluorescence probes. One of the easiest labeling strategies is to make a fusion enzyme with a fluorescent protein (e.g., the green fluorescence protein, GFP). The labeling ratio can be very high, if the linker peptide between the protein and GFP is not cleaved by proteases. But for cellulase analysis, the size of GFP is almost same as the size of the CD. Thus, it has the possibility to inhibit the binding. The other method of fluorescence labeling is conjugation with small dyes. Many kinds of combinations of dyes and functional groups are commercially available. Cy3-maleimide is used for labeling of cellulase, in that a free cysteine residue is introduced far from the expected cellulose-binding surface. Cy3 itself does not bind to cellulose; thus, labeling will not affect the binding properties of cellulase. Because cellulases work outside the cell, an unexpected reaction with an intrinsic free cysteine rarely happens. Therefore, conjugation with a maleimide group is easier for specific labeling than using isothiocyanate and

N-hydroxysuccinimide ester groups that react with amide groups. After labeling with Cy3, the unreacted dye should be completely removed with size exclusion chromatography or ultrafiltration to calculate the labeling ratio of the enzyme. This labeling ratio is needed to normalize the observed k_{on} value. Cellulose crystals were stabilized on glass for observation (usually, cover glass with a thickness of 0.12–0.17 mm is used) by spin coating. The glass is treated with 10 M KOH overnight and carefully washed with ultrapure water to remove fluorescence by debris. If a His6-tag is used for enzyme purification, it should be removed by protease treatment before observation. Histidine residues have positive charges at acidic pH and cause non-specific binding to the glass surface.

Total internal reflection fluorescence microscopy was used to observe the fluorescence from single dye molecules. Illumination by total internal reflected light can excite the molecules just near the glass surface (~200 nm). Therefore, background intensity from unbound molecules is kept low, and only bound molecules on the crystal surface are observed. Observation conditions for k_{on} and k_{off} analysis are 5 fps with $0.14 \mu\text{W}/\mu\text{m}^2$ of laser power (532 nm) to visualize the fast dissociation events and long binding events without photobleaching. The photobleaching time of Cy3 in 50 mM sodium acetate buffer, pH 5.0, at 25 °C is 18.8 ± 0.8 s under these observation conditions. For observation of single molecules, 25 to 250 pM of 20 μl enzyme solution is dropped on the glass, and cellulose fibrils are stained by 10 nM labeled enzyme. A movie of binding and dissociation is overlaid with the stained cellulose image using ImageJ software, and the number of bound molecules on each crystal and the binding times of each molecule are counted during the observation time. Lengths of cellulose fibrils are calculated from the length and pixel size in the stained image. The value of k_{on} is defined by the number of bound molecules per concentration of enzyme (M), standard length of the fibril (μm), and analyzed time (s). The value of k_{on} for the target enzyme is estimated from the peak of a Gaussian fit to the distribution of k_{on} for each fibril. The value of k_{off} is obtained by fitting with exponential decays to the distribution of the binding time of the molecules. Movies for the analysis of moving velocities and processivity are recorded at 0.5 fps with $0.28 \mu\text{W}/\mu\text{m}^2$ laser power to improve the position precision. The values of precision on the x- and y-axis are 6 to 8 nm, and the photobleaching time is 15.0 ± 0.7 s. Moving distances and times of molecules that move more than three frames along with cellulose are analyzed. Velocity, moving time, and processivity are analyzed with the same method used for HS-AFM observation.

To understand the complete reaction cycle of cellulase, not only the velocity of processive movement (k_{tr}) but also the rate constants of binding (k_{on}) and dissociation (k_{off}) should be analyzed. In HS-AFM observation, the total number of binding molecules is difficult to count, due to the limited field of view and non-specific binding of enzymes to graphite or the hydrophobic, coated mica surface. TrCel7A and TrCel6A have been observed by single-molecule fluorescence microscopy (Shibafuji et al. 2014; Nakamura et al. 2016). The results of the kinetic constant analysis are summarized in the following subsections.

10.4.1 Analysis of the Binding and Dissociation Rate Constants of Cellulose

Distributions of binding constants of both TrCel7A and TrCel6A showed multiple peaks (Fig. 10.6). Peak values are roughly quantized in both cases, due to the bundled forms of fibrils. By HS-AFM observation of the cellulose crystals, bundles of crystals were observed. The width of single crystals of cellulose I_{α} and III_1 that are the different shapes of crystals were 24 nm and 21 nm, respectively. Thus, bundles of cellulose were not resolved by fluorescence microscopy (special resolution is $\sim \lambda/2$), and k_{on} values might show quantized values. First peaks of k_{on} (corresponding to the single crystals) for cellulose I_{α} of TrCel7A and TrCel6A were $7.3 \times 10^8 \pm 0.3 \times 10^8 \text{ M}^{-1}\mu\text{m}^{-1}\text{s}^{-1}$ and $7.5 \times 10^8 \pm 0.3 \times 10^8 \text{ M}^{-1}\mu\text{m}^{-1}\text{s}^{-1}$, respectively. These two

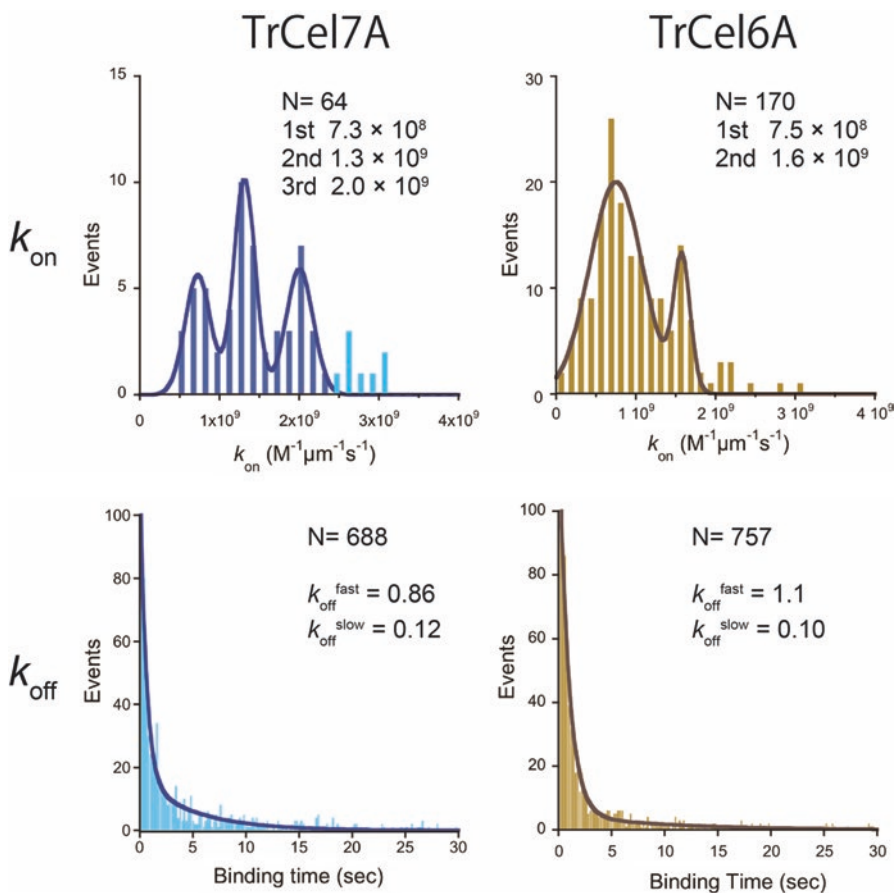


Fig. 10.6 k_{on} and k_{off} of TrCel7A and TrCel6A for cellulose I_{α} measured by single-molecule fluorescence microscopy

enzymes both consist of the CBD, a linker, and the CD. These similar values of k_{on} represent the similarities of the domain structures. When the k_{on} values of the CD, CBD-linker, and CBD of TrCel6A are compared with the value for the whole structure of TrCel6A, the values of the CD ($5.2 \times 10^7 \pm 0.4 \times 10^7 \text{ M}^{-1}\mu\text{m}^{-1}\text{s}^{-1}$) and the CBD ($5.6 \times 10^7 \pm 0.2 \times 10^7 \text{ M}^{-1}\mu\text{m}^{-1}\text{s}^{-1}$) were less than one tenth of the whole enzyme. Although that of the CBD-linker was $3.9 \times 10^8 \pm 0.05 \times 10^8 \text{ M}^{-1}\mu\text{m}^{-1}\text{s}^{-1}$, that is just a half of the full-length TrCel6A. These results mean that the linker region is very important for the initial interaction with the cellulose surface. The linker region of cellobiohydrolases from fungi is comprised of serine- and threonine-rich sequences and highly O-glycosylated. The role of glycosylation has been thought to be for protection from proteolysis. Recently, the interaction between sugars of the linker and the cellulose crystal has been proposed by molecular dynamics simulations (Payne et al. 2013). The results of the k_{on} analysis by single-molecule fluorescence microscopy are highly consistent with this hypothesis.

Distributions of the binding time for TrCel7A and TrCel6A on cellulose I_α were fitted with a double exponential decay (Fig. 10.6). The values of k_{off} and their ratios of TrCel7A are $0.12 \pm 0.01/\text{s}$ (48%) and $0.86 \pm 0.03/\text{s}$ (58%). Those of TrCel6A are $0.10 \pm 0.02/\text{s}$ (30%) and $1.1 \pm 0.03/\text{s}$ (70%). These results mean that they have at least two binding modes, with different binding energies for the cellulose surface. There are many possibilities for multiple binding modes. Expected reasons are, for example, binding with the CBD and the CD (nonproductive and productive), binding to the crystal region or amorphous region, and differences in the binding surfaces (hydrophobic and hydrophilic). The most probable one is differences at the binding surface. For observation, highly crystalline cellulose, purified from green algae, was used. The crystallinity of cellulose was more than 99%, indicating that binding to the amorphous region is rare. Additionally, only the CBD showed two binding modes with similar k_{off} values and ratios to the whole protein, meaning the double domain structure is not the main reason.

10.4.2 Analysis of Velocity and Processivity of Cellulase by Single-Molecule Fluorescence Microscopy

TrCel6A had been thought of as a processive cellulase from biochemical assays and electron microscopy observation, but processive movement was not found in HS-AFM observation. Therefore, the processive movement of TrCel6A was monitored with improved position precision. As a result, molecules moving along with cellulose fibrils were found, and the distribution of velocities was fitted by two Gaussian functions (peaks at $8.8 \pm 5.5 \text{ nm/s}$ and $34.9 \pm 16.3 \text{ nm/s}$), as shown in Fig. 10.7. To determine the velocity of processive movement, an inactive mutant of TrCel6A (D221A) was also observed in the same way. The distribution of velocities of the inactive mutant showed a single peak at $35.5 \pm 17.4 \text{ nm/s}$. Moving times of fast-moving TrCel6A and inactive mutant are almost less than 10 s, but that of

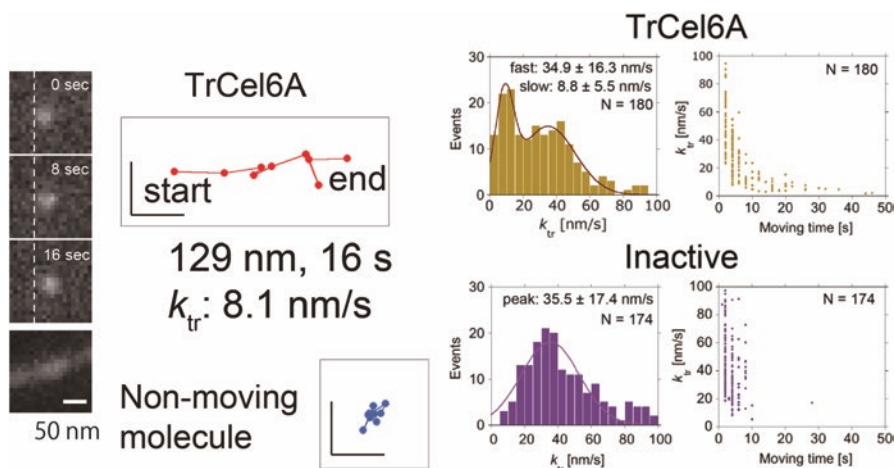


Fig. 10.7 Trajectory and velocity of TrCel6A measured by single-molecule fluorescence microscopy

slowly-moving TrCel6A was longer than 10 s. Distributions of moving times of long movement were fitted with a single exponential decay with a time constant of 7.7 s. When the step size was estimated as 1 nm, the processivity was calculated as 68 ± 42 . Furthermore, the distribution of velocity of the CD was fitted with a Gaussian distribution with peak at 39.2 ± 28.3 nm/s and moving times lower than 10 s, even though it was still active. From these results, it was shown that TrCel6A moves processively at 8.8 nm/s for 68 times, and the CBD-linker increases the processivity in the interaction with cellulose.

10.5 Conclusions and Future Directions

In this chapter, visualization of protonation states and the proton pathway of cellulase by neutron crystallography and visualization of kinetic elementary steps of processive cellulases by HS-AFM and single-molecule fluorescence microscopy were introduced. These methods are very useful to directly analyze the functional structure and dynamic motion of a cellulase on the surface of cellulose.

One of the good targets for the future study of structural analysis of cellulases is the catalytic mechanism of GH6 enzymes. TrCel6A is the most historical cellulase, but its catalytic mechanism is still under discussion, because the possible catalytic base is far from the putative catalytic acid residue. To determine the catalytic base, protonation state analysis by neutron crystallography is helpful. Another useful method is the characterization of processive cellobiohydrolases, as linear molecular motors. In the case of other linear motors, like kinesin-1 and myosin, distribution of step sizes and dwell times during pauses have been reported (Svoboda et al. 1993;

Kitamura et al. 1999), and their moving mechanisms have been discussed. HS-AFM could not resolve the single steps of TrCel7A, because the frame rate is still not fast enough. The expected step size of cellobiohydrolases is 1 nm, and the step size of TrCel7A was reported as 1.3 ± 0.7 nm, using optical tweezers with $1.25 \mu\text{m}$ polystyrene beads (Brady et al. 2015). The moving power of TrCel7A was shown as more than 20 pN, but the observed velocities of TrCel7A were less than one tenth of that in HS-AFM observation. Thus, it is difficult to discuss kinetics and moving mechanisms. For further analysis of the moving mechanism of cellulases, single-molecule observation with higher precision and time resolution and lower inhibition to movement, e.g., using a gold nanoparticle as a probe (Isojima et al. 2016), is needed. Furthermore, the difference between cellulase and chitinase is interesting. Chitinase A from a bacteria *Serratia marcescens* (SmChiA) hydrolyzes and moves on chitin crystals that have a similar structure to cellulose. The k_{on} and k_{off} of SmChiA were both about 3 times larger than those of TrCel7A, indicating a similar (K_d) (Nakamura et al. 2018). However, a moving velocity of 70.5 nm/s was observed in SmChiA using HS-AFM that was approximately ten times faster than that of TrCel7A (Igarashi et al. 2014). When the moving mechanism of cellulase is revealed, the big difference in moving velocities will be explained. At last, the synergistic effect between GH7 and GH6 cellobiohydrolases that move in opposite directions of each other is the most mysterious topic. Localization and movement of each enzyme should be analyzed at the same time using multicolor imaging techniques.

Acknowledgments This study was supported by Grants-in-Aid for Scientific Research from the Ministry of Education, Culture, Sports, Science, and Technology, Japan [grant numbers JP17K19213, JP16H00789, JP16H00858, and JP15H04366 to R. I., JP15H06898, JP17K18429, and JP17H05899 to A. N.], Advanced Technology Institute Research Grants 2015 (RG2709 to A.N.).

References

- Ando T (2013) High-speed atomic force microscopy (AFM). In: Encyclopedia of biophysics. vol Chapter 478. Springer, Berlin/Heidelberg/Berlin/Heidelberg, pp 984–987. https://doi.org/10.1007/978-3-642-16712-6_478
- Ando T (2017) Directly watching biomolecules in action by high-speed atomic force microscopy. Biophys Rev 9(4):421–429. <https://doi.org/10.1007/s12551-017-0281-7>
- Brady SK, Sreelatha S, Feng Y, Chundawat SPS, Lang MJ (2015) Cellobiohydrolase 1 from *Trichoderma reesei* degrades cellulose in single cellobiose steps. Nat Commun 6:10149. <https://doi.org/10.1038/ncomms10149>
- Chanzy H, Henrissat B (1985) Unidirectional degradation of valonia cellulose microcrystals subjected to cellulase action. FEBS Lett 184(2):285–288. [https://doi.org/10.1016/0014-5793\(85\)80623-2](https://doi.org/10.1016/0014-5793(85)80623-2)
- Davies G, Henrissat B (1995) Structures and mechanisms of glycosyl hydrolases. Structure 3(9):853–859. [https://doi.org/10.1016/S0969-2126\(01\)00220-9](https://doi.org/10.1016/S0969-2126(01)00220-9)
- Igarashi K, Koivula A, Wada M, Kimura S, Penttila M, Samejima M (2009) High speed atomic force microscopy visualizes processive movement of *Trichoderma reesei* cellobiohydrolase I on crystalline cellulose. J Biol Chem 284(52):36186–36190. <https://doi.org/10.1074/jbc.M109.034611>

- Igarashi K, Uchihashi T, Koivula A, Wada M, Kimura S, Okamoto T, Penttila M, Ando T, Samejima M (2011) Traffic jams reduce hydrolytic efficiency of cellulase on cellulose surface. *Science* 333(6047):1279–1282. <https://doi.org/10.1126/science.1208386>
- Igarashi K, Uchihashi T, Uchiyama T, Sugimoto H, Wada M, Suzuki K, Sakuda S, Ando T, Watanabe T, Samejima M (2014) Two-way traffic of glycoside hydrolase family 18 processive chitinases on crystalline chitin. *Nat Commun* 5:1–7. <https://doi.org/10.1038/ncomms4975>
- Iino R, Iida T, Nakamura A, E-i S, You H, Sako Y (2017) Single-molecule imaging and manipulation of biomolecular machines and systems. *Biochim Biophys Acta* S0304-4165(17):30253–30252. <https://doi.org/10.1016/j.bbagen.2017.08.008>
- Imai T, Boisset C, Samejima M, Igarashi K, Sugiyama J (1998) Unidirectional processive action of cellobiohydrolase Cel7A on Valonia cellulose microcrystals. *FEBS Lett* 432(3):113–116. [https://doi.org/10.1016/S0014-5793\(98\)00845-X](https://doi.org/10.1016/S0014-5793(98)00845-X)
- Isojima H, Iino R, Niitani Y, Noji H, Tomishige M (2016) Direct observation of intermediate states during the stepping motion of kinesin-1. *Nat Chem Biol* 12(4):290–297. <https://doi.org/10.1038/nchembio.2028>
- Jalak J, Kurasin M, Teugas H, Valjamae P (2012) Endo-exo synergism in cellulose hydrolysis revisited. *J Biol Chem* 287(34):28802–28815. <https://doi.org/10.1074/jbc.M112.381624>
- Jullian V, de Vaux A, Millet L, Fonty G (1999) Identification of *Ruminococcus flavefaciens* as the predominant cellulolytic bacterial species of the equine cecum. *Appl Environ Microbiol* 65(8):3738–3741
- Kitamura K, Tokunaga M, Iwane AH, Yanagida T (1999) A single myosin head moves along an actin filament with regular steps of 5.3 nanometres. *Nature* 397(6715):129–134. <https://doi.org/10.1038/16403>
- Kodera N, Uchida K, Ando T, Aizawa S-I (2015) Two-ball structure of the flagellar hook-length control protein FliK as revealed by high-speed atomic force microscopy. *J Mol Biol* 427(2):406–414. <https://doi.org/10.1016/j.jmb.2014.11.007>
- Kodera N, Yamamoto D, Ishikawa R, Ando T (2010) Video imaging of walking myosin V by high-speed atomic force microscopy. *Nature* 468(7320):72–76. <https://doi.org/10.1038/nature09450>
- Kusaka K, Hosoya T, Yamada T, Tomoyori K, Ohhara T, Katagiri M, Kurihara K, Tanaka I, Niimura N (2013) Evaluation of performance for IBARAKI biological crystal diffractometer iBIX with new detectors. *J Synchrotron Radiat* 20(6):994–998. <https://doi.org/10.1107/S0909049513021845>
- Leschine SB (1995) Cellulose degradation in anaerobic environments. *Annu Rev Microbiol* 49(1):399–426. <https://doi.org/10.1146/annurev.mi.49.100195.002151>
- Lombard V, Ramulu HG, Drula E, Coutinho PM, Henrissat B (2014) The carbohydrate-active enzymes database (CAZy) in 2013. *Nucleic Acids Res* 42(D1):D490–D495. <https://doi.org/10.1093/nar/gkt1178>
- McCarter JD, Stephen Withers G (1994) Mechanisms of enzymatic glycoside hydrolysis. *Curr Opin Struct Biol* 4(6):885–892. [https://doi.org/10.1016/0959-440X\(94\)90271-2](https://doi.org/10.1016/0959-440X(94)90271-2)
- McMaster WH, Del Grande NK, Mallett JH, Hubbell JH (1969) Compilation of X-ray cross sections. Lawrence Livermore National Laboratory Report UCRL-50174
- Nakamura A, Ishida T, Fushinobu S, Kusaka K, Tanaka I, Inaka K, Higuchi Y, Masaki M, Ohta K, Kaneko S, Niimura N, Igarashi K, Samejima M (2013a) Phase-diagram-guided method for growth of a large crystal of glycoside hydrolase family 45 inverting cellulase suitable for neutron structural analysis. *J Synchrotron Radiat* 20(6):859–863. <https://doi.org/10.1107/S0909049513020943>
- Nakamura A, Ishida T, Kusaka K, Yamada T, Fushinobu S, Tanaka I, Kaneko S, Ohta K, Tanaka H, Inaka K, Higuchi Y, Niimura N, Samejima M, Igarashi K (2015) “Newton’s cradle” proton relay with amide-imidic acid tautomerization in inverting cellulase visualized by neutron crystallography. *Sci Adv* 1(7):e1500263–e1500263. <https://doi.org/10.1126/sciadv.1500263>
- Nakamura A, Tasaki T, Ishiwata D, Yamamoto M, Okuni Y, Visootsat A, Maximilien M, Noji H, Uchiyama T, Samejima M, Igarashi K, Iino R (2016) Single-molecule imaging analysis of binding, processive Movement, and dissociation of cellobiohydrolase *Trichoderma reesei*

- Cel6A and its domains on crystalline cellulose. *J Biol Chem* 291(43):22404–22413. <https://doi.org/10.1074/jbc.M116.752048>
- Nakamura A, Tasaki T, Okuni Y, Song C, Murata K, Kozai T, Hara M, Sugimoto H, Suzuki K, Watanabe T, Uchihashi T, Noji H, Iino R (2018) Rate constants, processivity, and productive binding ratio of chitinase A revealed by single-molecule analysis. *Phys Chem Chem Phys* 20(5):3010–3018. <https://doi.org/10.1039/c7cp04606e>
- Nakamura A, Tsukada T, Auer S, Furuta T, Wada M, Koivula A, Igarashi K, Samejima M (2013b) The tryptophan residue at the active site tunnel entrance of *Trichoderma reesei* cellobiohydrolase Cel7A is important for initiation of degradation of crystalline cellulose. *J Biol Chem* 288(19):13503–13510. <https://doi.org/10.1074/jbc.M113.452623>
- Nakamura A, Watanabe H, Ishida T, Uchihashi T, Wada M, Ando T, Igarashi K, Samejima M (2014) Trade-off between processivity and hydrolytic velocity of cellobiohydrolases at the surface of crystalline cellulose. *J Am Chem Soc* 136(12):4584–4592. <https://doi.org/10.1021/ja4119994>
- Ogata H, Nishikawa K, Lubitz W (2015) Hydrogens detected by subatomic resolution protein crystallography in a [NiFe] hydrogenase. *Nature* 520(7548):571–574. <https://doi.org/10.1038/nature14110>
- Payne CM, Resch MG, Chen L, Crowley MF, Himmel ME, Taylor LE II, Sandgren M, Ståhlberg J, Stals I, Tan Z, Beckham GT (2013) Glycosylated linkers in multimodular lignocellulose-degrading enzymes dynamically bind to cellulose. *Proc Natl Acad Sci U S A* 110(36):14646–14651. <https://doi.org/10.1073/pnas.1309106110>
- Shibafuji Y, Nakamura A, Uchihashi T, Sugimoto N, Fukuda S, Watanabe H, Masahiro S, Toshio A, Hiroyuki N, Koivula A, Kiyohiko I, Ryota I (2014) Single-molecule imaging analysis of elementary reaction steps of *Trichoderma Reesei* cellobiohydrolase I (Cel7A) hydrolyzing crystalline cellulose I α and III. *J Biol Chem* 289(20):14056–14065. <https://doi.org/10.1074/jbc.M113.546085>
- Shibata M, Yamashita H, Uchihashi T, Kandori H, Ando T (2010) High-speed atomic force microscopy shows dynamic molecular processes in photoactivated bacteriorhodopsin. *Nat Nanotechnol* 5(3):208–212. <https://doi.org/10.1038/nnano.2010.7>
- Štursová M, Žifčáková L, Leigh MB, Burgess R, Baldrian P (2012) Cellulose utilization in forest litter and soil: identification of bacterial and fungal decomposers. *FEMS Microbiol Ecol* 80(3):735–746. <https://doi.org/10.1111/j.1574-6941.2012.01343.x>
- Svoboda K, Schmidt CF, Schnapp BJ, Block SM (1993) Direct observation of kinesin stepping by optical trapping interferometry. *Nature* 365(6448):721–727. <https://doi.org/10.1038/365721a0>
- Uchihashi T, Iino R, Ando T, Noji H (2011) High-speed atomic force microscopy reveals rotary catalysis of rotorless F1-ATPase. *Science* 333(6043):755–758. <https://doi.org/10.1126/science.1206333>
- Varley FS (1992) Neutron scattering lengths and cross section. *Neutron News* 3(3):26–37. <https://doi.org/10.1080/10448639208218770>
- Wood RKS (1960) Pectic and cellulolytic enzymes in plant disease. *Annu Rev Plant Physiol* 11(1):299–322. <https://doi.org/10.1146/annurev.pp.11.060160.001503>